ARTICLES

Journal of Semiconductors
(2023) 44, 052901
doi: 10.1088/1674-4926/44/5/052901

Squeezed state generation using cryogenic InP HEMT nonlinearity

Ahmad Salmanogli†

Engineering Faculty, Electrical and Electronic Department, Cankaya University, Ankara, Turkey

Abstract: This study focuses on generating and manipulating squeezed states with two external oscillators coupled by an InP HEMT operating at cryogenic temperatures. First, the small-signal nonlinear model of the transistor at high frequency at 5 K is analyzed using quantum theory, and the related Lagrangian is theoretically derived. Subsequently, the total quantum Hamiltonian of the system is derived using Legendre transformation. The Hamiltonian of the system includes linear and nonlinear terms by which the effects on the time evolution of the states are studied. The main result shows that the squeezed state can be generated owing to the transistor's nonlinearity; more importantly, it can be manipulated by some specific terms introduced in the nonlinear Hamiltonian. In fact, the nonlinearity of the transistors induces some effects, such as capacitance, inductance, and second-order transconductance, by which the properties of the external oscillators are changed. These changes may lead to squeezing or manipulating the parameters related to squeezing in the oscillators. In addition, it is theoretically derived that the circuit can generate two-mode squeezing. Finally, second-order correlation (photon counting statistics) is studied, and the results demonstrate that the designed circuit exhibits antibunching, where the quadrature operator shows squeezing behavior.

Key words: quantum theory; squeezed state; cryogenic low noise amplifier; InP HEMT

Citation: A Salmanogli, Squeezed state generation using cryogenic InP HEMT nonlinearity[J]. *J. Semicond.*, 2023, 44(5), 052901. https://doi.org/10.1088/1674-4926/44/5/052901

1. Introduction

The squeezing state and its applications have been developed recently[1–3]. It has been shown that squeezing originates from nonlinearity effects in any system[1–7]. Different approaches and systems have been employed to generate squeezed states[3–5]. For instance, phase conjugate mirrors using four-wave mixing interactions have been applied to create a squeezed state[1, 8]. Another important option is using a parametric amplifier, in which three-wave mixing is used to generate the squeezed state[5, 7]. In addition, by controlling the spontaneous emission, a two-photon laser is applied to produce a squeezed state[1]. Moreover, atomic interaction with an optical wave can produce a nonlinear medium, creating a squeezed state. Additionally, other phenomena, such as third-order nonlinearity of the wave propagation in the optical fiber, can generate a squeezed state[7]. In quantum applications, the squeezed state is very important because it introduces less fluctuation in one quadrature phase than the coherent state, which is very similar to the classical state[9–13]. Quantum fluctuation in a coherent state is equal to zero-point fluctuation, in which the standard quantum limits noise reduction in a signal[1, 14]. Therefore, the noise fluctuation can be reduced below the standard limit when the system is in a squeezed state[14]. There is no classical analog for the squeezed state, and this state, in contrast to the coherent state that shows Poisson photon counting (photon bunching) statistics, may show sub-Poisson photon counting (photon antibunching)[1, 2, 13, 14]. In other words, there is no direct connection between squeezing and photon antibunching, but each is a nonclassical phenomenon[1, 3, 13]. For some quantum applications, such as quantum radar and quantum sensors[15–20], the noise effect is critical when the system tries to detect low-level backscattering signals. For signal detection, the received signals, which have minimal levels, can be easily affected by noise. Therefore, to control and limit the noise, it is necessary to prepare the key subsystems, such as the low-noise amplifier (LNA) and detector, to operate in the squeezed state by which the noise can be reduced below the zero-point fluctuation. The LNA is an electronic amplifier generally designed to amplify low-level signals while simultaneously keeping the noise at a very low level[21–24]. Today, a cryogenic LNA has been designed to operate at very low temperatures around 5 K, to strongly limit noise. So due to this fact, cryogenic LNAs are so popular in quantum applications[24–29].

With the knowledge of the points mentioned above, in this work, we attempt to design a circuit containing two external oscillators coupled to an InP high electron mobility transistor (HEMT) operating at cryogenic temperature to create the squeezed states. This type of transistor was selected because HEMT technology does not have a strong effect from freeze-out at a cryogenic temperature[24–27]. The designed circuit can be considered a core circuit for an LNA used in front-end transceivers to amplify faint signals. In this study, the nonlinear properties of the cryogenic InP HEMT play a key role, and we discuss how emerging nonlinearity can affect the state of the coupling oscillators. Additionally, a critical point will be addressed, which relates to the trade-off between squeezing generated by the nonlinear properties of the transistor and the degradation of the produced state because of the damping created by the transistor's internal circuits.

Correspondence to: A Salmanogli, salmanogli@cankaya.edu.tr
Received 11 NOVEMBER 2022; Revised 2 JANUARY 2023.

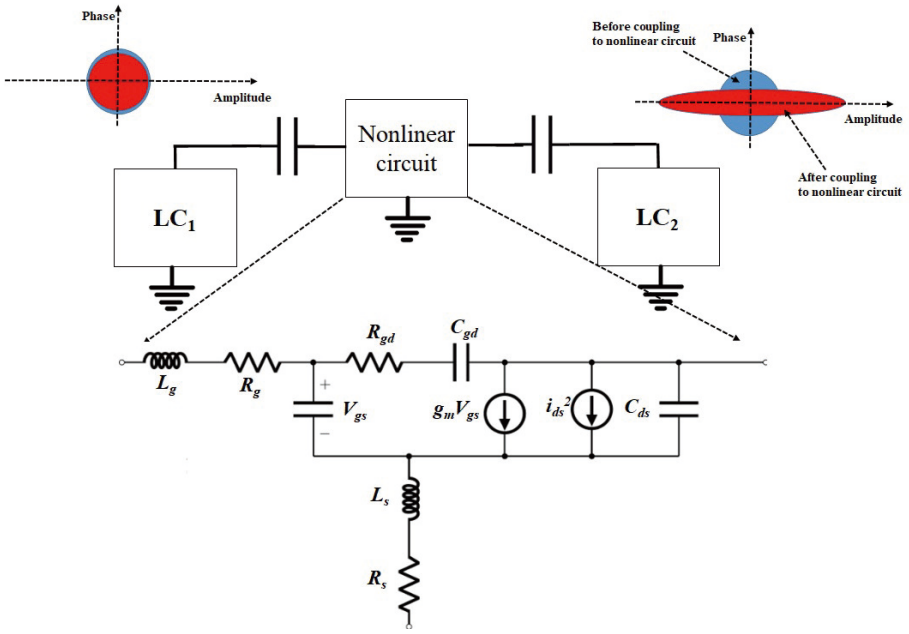

Fig. 1. (Color online) Schematic of the system containing two external oscillators coupling through a nonlinear device, inset figure: nonlinear device internal circuit.

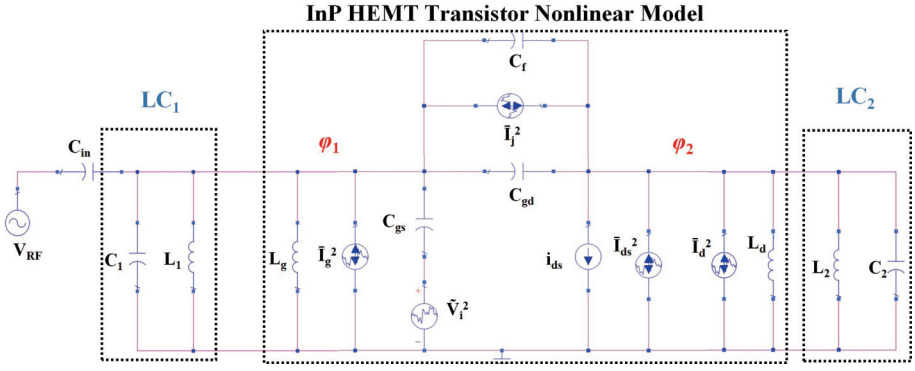

Fig. 2. (Color online) Complete system model; LC_1 coupling to LC_2 through InP HEMT transistor operating at 5 K.

2. Theoretical and backgrounds

2.1. System description

The circuit is schematically shown in Fig. 1, which shows two LC oscillators (resonators) coupled to each other through a nonlinear device (depicted in the inset figure). As mentioned in the previous section, the main goal is to create a squeezing state in a low-noise amplifier (LNA), which is essential in quantum sensing applications[15, 16, 25]. In fact, if such a circuit is prepared in the squeezing state, it helps minimize the noise effect. This implies that the performance of the cryogenic LNA, at which the noise strongly limits the operation, is enhanced. Therefore, the circuit shown in Fig. 1 is designed. In this circuit, the transistor is used as a nonlinear element, and the state of the oscillators may exhibit squeezing. It has been theoretically shown that nonlinearity arises because the transistor can be expressed as a nonlinear capacitor, inductor coupling to the second oscillator, and second-order transconductance (g_{m2_N}). These factors are defined in detail in the next section and can intensely manipulate the state of the oscillators to create squeezing. Additionally, Fig. 1 schematically reveals that only the second oscillator can generate squeezing in the state; this important point will be discussed in detail later. Nonetheless, we theoretically demonstrate that coupling oscillators can generate two-mode squeezing.

The high-frequency model of an InP HEMT transistor[25, 27] coupled with two oscillators is shown in Fig. 2. Some elements in the nonlinear transistor model are created owing to the high-frequency effect, such as C_{gs}, C_{gd}, L_g, and L_d and some other components, such as resistors, as shown in Fig. 1, are created to address the thermal loss in the circuit. These elements are sources of thermal noise in the transistor, and their effects are shown as voltage and current noise sources in Fig. 2. In fact, $\bar{I}_g^2$, $\bar{I}_j^2$, $\bar{I}_d^2$, and $\bar{V}_i^2$ model the thermal noise of R_g, R_{gd}, R_{ds}, and R_{gs}, respectively. A noise model is applied to the circuit to demonstrate the effects of the contributed resistors. Additionally, we ignored the Ls effect and merged R_s with R_{gs} to simplify algebra. In the circuit, i_{ds} and $\bar{I}_{ds}^2$ are the dependent current sources containing the transistor's nonlinearity and related thermal noise, which is a critical factor in generating noise. Finally, C_f, C_{in}, V_{RF}, φ_1, and φ_2 are the feedback capacitor and coupling capacitors used to separate the input signal from the DC signals, input signal, and node flux for the input and output nodes, respectively. This circuit is wholly analyzed using quantum theory, and we will attempt to derive the contributed Lagrangian initially; then, the total Hamiltoni-

Table 1. Values for the small signal model of the 2 × 50 μm InP HEMT at 5 K [31-33].

	Stands for	Value
R_g	Gate resistance	0.3 Ω
L_g	Gate inductance	75 pH
L_d	Drain inductance	70 pH
C_{gs}	Gate–source capacitance	69 fF
C_{ds}	Drain–source capacitance	29 fF
C_{gd}	Gate–drain capacitance	19 fF
R_{gs}	Gate-source resistance	4 Ω
R_{gd}	Gate–drain resistance	35 Ω

an of the system is examined, in which the factors that cause the squeezing in the state will be addressed.

2.2. Designed system Hamiltonian

This section analyzes the circuit shown in Fig. 2 using the full quantum theory. As shown in the circuit, it includes all noises that can affect the signals, such as the thermal noises generated by the dependent current source and resistors in the circuit. The data for the nonlinear model of the InP HEMT operating at cryogenic temperatures are listed in Table 1. First, we theoretically derive the total Lagrangian of the system to obtain the quantum properties of the circuit illustrated in Fig. 2. For the analysis, the coordinate variables are defined as φ_1 and φ_2 (node flux), as shown in Fig. 2, and the momentum conjugate variables are defined by Q_1 and Q_2 (loop charge). The total Lagrangian of the circuit is derived as[29]:

$$\begin{aligned} L_c =& \frac{C_{in}}{2}(\dot{\varphi}_1 - V_{RF})^2 + \frac{C_1}{2}\dot{\varphi}_1^2 - \frac{1}{2L_1}\varphi_1^2 + \overline{I_g^2}\varphi_1 \\ &+ \frac{C_{gs}}{2}\left(\dot{\varphi}_1 - \overline{V_i^2}\right)^2 + \frac{C_{gd}+C_f}{2}(\dot{\varphi}_1 - \dot{\varphi}_2)^2 + i_{ds}\varphi_1 \\ &+ \left(\overline{I_{ds}^2} + \overline{I_d^2}\right)\varphi_2 + \frac{C_2}{2}\dot{\varphi}_2^2 - \frac{1}{2L_2}\varphi_2^2 + \overline{I_j^2}(\varphi_2 - \varphi_1). \end{aligned} \tag{1}$$

In this equation, the dependent current source is defined as $i_{ds} = g_m V_{gs} + g_{m2} V_{gs}{}^2 + g_{m3} V_{gs}{}^3$ [22,30], where g_m is the intrinsic transconductance of the transistor and g_{m2} and g_{m3} are the second-and third-order transconductance. These terms (g_{m2}, g_{m3}) bring nonlinearity to the circuit. Moreover, thermally generated noises by the resistors and the current source are defined as $\overline{I_g^2} = 4K_BT/R_g$, $\overline{I_d^2} = 4K_BT/R_d$, $\overline{I_j^2} = 4K_BT/R_j$, $\overline{I_{ds}^2} = 4K_BT\gamma g_m$, and $\overline{I_i^2} = 4K_BT/R_i$, where K_B, T, and γ respectively are the Boltzmann constant and operational temperature, and empirical constant[29]. The noise bandwidth is supposed to be very wide (1 Hz). Using the Legendre transformation[14, 29], one can theoretically derive the classical Hamiltonian of the circuit. For this, it is necessary to calculate the momentum conjugate variables using $Q_i = \partial L_c/\partial(\partial\varphi_i/\partial t)$ for i = 1, 2 represented as:

$$\begin{aligned} Q_1 =& \left(C_{in} + C_1 + C_{gs} + C_f + C_{gd}\right)\dot{\varphi}_1 - \left(C_f + C_{gd}\right)\dot{\varphi}_2 \\ &- C_{in}V_{RF} + g_m\varphi_2 + 2g_{m2}\varphi_2\dot{\varphi}_1 + 3g_{m3}\varphi_2\dot{\varphi}_1^2 - C_{gs}\overline{V_i^2}, \\ Q_2 =& \left(C_2 + C_f + C_{gd}\right)\dot{\varphi}_2 - \left(C_f + C_{gd}\right)\dot{\varphi}_1. \end{aligned} \tag{2}$$

Applying Legendre transformation, the classical Hamiltonian is expressed as:

$$\begin{aligned} H_c =& \left\{\frac{C_A}{2}\dot{\varphi}_1^2 + \frac{1}{2L_1}\varphi_1^2 + \frac{C_B}{2}\dot{\varphi}_2^2 + \frac{1}{2L_2}\varphi_2^2\right\} \\ &+ \left\{-C_c\dot{\varphi}_1\dot{\varphi}_2 + g_{m2}\varphi_2\dot{\varphi}_1^2 + 2g_{m3}\varphi_2\dot{\varphi}_1^3\right\} \\ &+ \left\{-\varphi_1\left(\overline{I_g^2} - \overline{I_j^2}\right) - \varphi_2\left(\overline{I_d^2} + \overline{I_j^2} + \overline{I_{ds}^2}\right) - \frac{C_{gs}}{2}\overline{V_i^2}\right\}, \end{aligned} \tag{3}$$

where $C_A = C_{in} + C_1 + C_{gs} + C_f + C_{gd}$, $C_B = C_{gd} + C_f + C_2$, and $C_C = C_f + C_{gd}$. In Eq. (3), the first term relates to the LC resonance Hamiltonian affected by the coupling elements. It is clearly shown that C_A and C_B are affected due to the transistor's internal circuit. The second term contributes to the linear and nonlinear coupling between the LC resonators and the nonlinear circuit. Finally, the third term defines the noise effect in the system, which is originally generated by the transistor nonlinearity in the circuit. In the following, using Eq. (2), one can express the first derivative of the coordinate variables ($\partial\varphi_i/\partial t$) in terms of the momentum conjugates (Q_i) represented in the matrix form as:

$$\begin{bmatrix} \dot{\varphi}_1 \\ \dot{\varphi}_2 \end{bmatrix} = \frac{1}{C_M{}^2}\left\{\begin{bmatrix} C_B & C_C \\ C_C & C_A + C_N \end{bmatrix}\begin{bmatrix} Q_1 \\ Q_2 \end{bmatrix} + \begin{bmatrix} C_B & C_C \\ C_C & C_A + C_N \end{bmatrix}\begin{bmatrix} C_{in} & 0 \\ 0 & 0 \end{bmatrix}\begin{bmatrix} V_{RF} \\ 0 \end{bmatrix} - \begin{bmatrix} C_B & C_C \\ C_C & C_A + C_N \end{bmatrix}\begin{bmatrix} 0 & g_m \\ 0 & 0 \end{bmatrix}\begin{bmatrix} \varphi_1 \\ \varphi_2 \end{bmatrix}\right\}, \tag{4}$$

where $C_M{}^2 = C_B(C_A + C_N) - C_C{}^2$ and $C_N = 2g_{m2}\varphi_{2\_dc} + 6g_{m3}\varphi_{2\_dc}(\partial\varphi_i/\partial t)|_{dc}$ is the capacitor generated due to the nonlinearity effect. In the following, we will show that this quantity strongly affects the coupled LC resonator's frequency and impedances, and consequently, the quantum properties of the LC resonators are severely influenced by C_N. By substitution of Eq. (4) into Eq. (3) one can derive the total Hamiltonian for the system; however, to study the design in detail and get to know about each factor's impact on the system, we initially use the linearization technique to linearize the nonlinear terms in the second term of Eq. (3). Thus, the linear Hamiltonian of the system is defined as:

$$H_L = \left\{\frac{1}{2C_{q1}}Q_1^2 + \frac{1}{2L_1}\varphi_1^2 + \frac{1}{2C_{q2}}Q_2^2 + \frac{1}{2L_2'}\varphi_2^2\right\} + \left\{\frac{1}{2C_{q1q2}}Q_1Q_2 + g_{12}Q_1\varphi_2 + g_{22}Q_2\varphi_2\right\} + \left\{V_{q1}Q_1 + V_{q2}Q_2 + I_{p2}\varphi_2 - \overline{I_{gs}^2}\varphi_1\right\}, \tag{5}$$

where C_{q1}, C_{q2}, C_{q1q2}, g_{12}, g_{22}, L_2', V_{q1}, V_{q2}, and I_{p2} are defined in Appendix A, and the dc terms are ignored for simplicity. In fact, these coefficients are essentially the function of g_m, C_N, C_C, and V_{RF} by which the nonlinearity effect of the transistor is emphasized. In other words, the nonlinearity created by the transistor induces some factors by which the properties of the coupling LC resonators are strongly affected. For instance, the LC resonator impedances are $Z_1 = (L_1/C_{q1})^{0.5}$, $Z_2 = (L_2'/C_{q2})^{0.5}$, and the associated frequencies are $\omega_1 = (L_1C_{q1})^{-0.5}$, $\omega_2 = (L_2'/C_{q2})^{-0.5}$. The relations show that the coupling oscillator's impedance and frequencies, especially the second LC become affected. Additionally, some terms in Eq. (2), such as Q_1Q_2, $Q_2\varphi_1$, and $Q_1\varphi_2$ show the coupling between oscillators in the circuit design. Also, in the third term in Eq. (5), some terms such as $V_{q1}Q_1$, $\overline{I_{gs}^2}\varphi_1$, $V_{g2}Q_2$, and $I_{p2}\varphi_2$ in the equation declare the RF source and thermal noise coupling to the contributed oscillators. In this equation, $\overline{I_{gs}^2} = \overline{I_g^2} - \overline{I_j^2}$. In

the following, one can derive the linear Hamiltonian in terms of annihilation and creation operators using the quantization procedure for the coordinates and the related momentum conjugates. The quadrature operators defined as $Q_1 = -\mathrm{i}(a_1 - a_1^+)(\hbar/2Z_1)^{0.5}$, $\varphi_1 = (a_1 + a_1^+)(\hbar Z_1/2)^{0.5}$ and $Q_2 = -\mathrm{i}(a_2 - a_2^+)(\hbar/2Z_2)^{0.5}$, $\varphi_2 = (a_2 + a_2^+)(\hbar Z_2/2)^{0.5}$, where (a_i, a_i^+) $i = 1, 2$ are the first and second oscillator's annihilation and creation operators. Thus, the linear Hamiltonian in terms of the ladder operators is given by:

$$H_{\mathrm{L}} = \left\{\hbar\omega_1\left(a_1^+a_1 + \frac{1}{2}\right) + \hbar\omega_2\left(a_2^+a_2 + \frac{1}{2}\right)\right\} + \left\{-\frac{\hbar}{2}\frac{1}{C_{q1q2}\sqrt{Z_1Z_2}}\left(a_1 - a_1^+\right)\left(a_2 - a_2^+\right) - \frac{i\hbar}{2}g_{12}\sqrt{\frac{Z_2}{Z_1}}\left(a_1 - a_1^+\right)\left(a_2 + a_2^+\right) - \frac{i\hbar}{2}g_{22}\left(a_2 - a_2^+\right)\left(a_2 + a_2^+\right)\right\}$$
$$+ \left\{-iV_{q1}\sqrt{\frac{\hbar}{2Z_1}}\left(a_1 - a_1^+\right) - iV_{q2}\sqrt{\frac{\hbar}{2Z_2}}\left(a_2 - a_2^+\right) + I_{p2}\sqrt{\frac{\hbar Z_2}{2}}\left(a_2 + a_2^+\right) - \overline{I_{gs}^2}\sqrt{\frac{\hbar}{2Z_2}}\left(a_1 + a_1^+\right)\right\}. \tag{6}$$

In the following, it is necessary to add the nonlinearity to the Hamiltonian and derive the total Hamiltonian containing the linear and nonlinear parts. The nonlinear terms in Eq. (3) can be re-written as:

$$H_N = \left\{g_{\mathrm{m2}} + 6g_{\mathrm{m3}}\dot{\varphi}_{1\_\mathrm{dc}}\right\}\varphi_2\dot{\varphi}_1^2. \tag{7}$$

Using Eq. (4), the nonlinear Hamiltonian is given by:

$$H_{\mathrm{N}} = g_{\mathrm{m2\_}N}\left[\left\{\frac{C_{\mathrm{B}}^2}{C_{\mathrm{M}}^4}\varphi_2Q_1^2 + \frac{C_{\mathrm{C}}^2}{C_{\mathrm{M}}^4}\varphi_2Q_2^2 + \frac{2C_{\mathrm{B}}C_{\mathrm{C}}}{C_{\mathrm{M}}^4}\varphi_2Q_2Q_1 - \frac{2g_{\mathrm{m}}C_{\mathrm{B}}^2}{C_{\mathrm{M}}^4}\varphi_2{}^2Q_1 - \frac{2g_{\mathrm{m}}C_{\mathrm{B}}C_{\mathrm{C}}}{C_{\mathrm{M}}{}^4}\varphi_2^2Q_2 + \frac{g_{\mathrm{m}}^2C_{\mathrm{B}}^2}{C_{\mathrm{M}}{}^4}\varphi_2^3\right\}_{\mathrm{NL}}\right.$$
$$\left.\times\left\{\frac{-2g_{\mathrm{m}}C_{\mathrm{B}}^2C_{\mathrm{in}}V_{\mathrm{RF}}}{C_{\mathrm{M}}^4}\varphi_2^2 + \frac{2C_{\mathrm{B}}^2C_{\mathrm{in}}V_{\mathrm{RF}}}{C_{\mathrm{M}}^4}Q_1\varphi_2 + \frac{2C_{\mathrm{B}}C_{\mathrm{C}}C_{\mathrm{in}}V_{\mathrm{RF}}}{C_{\mathrm{M}}^4}Q_2\varphi_2 + \frac{C_{\mathrm{B}}^2V_{\mathrm{in}}^2V_{\mathrm{RF}}^2}{C_{\mathrm{M}}^4}\varphi_2\right\}_L\right], \tag{8}$$

where $g_{\mathrm{m2\_}N} = g_{\mathrm{m2}} + 6g_{\mathrm{m3}}\left(\partial\varphi_i/\partial t\right)|_{\mathrm{dc}}$. The linear part of Eq. (8) can directly attach to Eq. (5) to make the modified linear Hamiltonian given by:

$$H_{\mathrm{L}} = \left\{\frac{1}{2C_{\mathrm{q1}}}Q_1^2 + \frac{1}{2L_1}\varphi_1^2 + \frac{1}{2C_{\mathrm{q2}}}Q_2^2 + \left(\frac{1}{2L_2'} + \frac{1}{2L_{2N}}\right)\varphi_2^2\right\} + \left\{\frac{1}{2C_{\mathrm{q1q2}}}Q_1Q_2 + \left(g_{12} + g_{12\mathrm{N}}\right)Q_1\varphi_2 + \left(g_{22} + g_{22\mathrm{N}}\right)Q_2\varphi_2\right\}$$
$$+ \left\{V_{\mathrm{q1}}Q_1 + V_{\mathrm{q2}}Q_2 + \left(I_{\mathrm{p2}} + I_{\mathrm{p2N}}\right)\varphi_2 - \overline{I_{\mathrm{gs}}^2}\varphi_1\right\}. \tag{9}$$

As can be clearly seen in Eq. (9), the nonlinear Hamiltonian can change the coupling between oscillators in the circuit. The most important factor is $g_{\mathrm{m2\_N}}$, which manipulates the coupling between different coordinates and their momentum conjugates. Additionally, the attachment from Eq. (8) to Eq. (5) changes the second resonator's inductance by a factor of L_{2N}. The term brought from nonlinearity (L_{2N}) manipulates the second resonator's impedance and frequency. Finally, the nonlinear terms of Eq. (8) are considered, and so, the total Hamiltonian of the system in terms of the ladder operators is given by:

$$H_{\mathrm{t}} = \left[\left\{\hbar\omega_1\left(a_1^+a_1 + \frac{1}{2}\right) + \hbar\omega_2\left(a_2^+a_2 + \frac{1}{2}\right)\right\}\right.$$
$$+ \left\{-\frac{\hbar}{2}\frac{1}{C_{\mathrm{q1q2}}\sqrt{Z_1Z_2}}\left(a_1 - a_1^+\right)\left(a_2 - a_2^+\right) - \frac{i\hbar}{2}g_{12}'\sqrt{\frac{Z_2}{Z_1}}\left(a_1 - a_1^+\right)\left(a_2 + a_2^+\right) - \frac{i\hbar}{2}g_{22}'\left(a_2 - a_2^+\right)\left(a_2 + a_2^+\right)\right\}$$
$$\left.+ \left\{-iV_{\mathrm{q1}}\sqrt{\frac{\hbar}{2Z_1}}\left(a_1 - a_1^+\right) - iV_{\mathrm{q2}}\sqrt{\frac{\hbar}{2Z_2}}\left(a_2 - a_2^+\right) + I_{p2}'\sqrt{\frac{\hbar Z_2}{2}}\left(a_2 + a_2^+\right) - \overline{I_{gs}^2}\sqrt{\frac{\hbar}{2Z_2}}\left(a_1 + a_1^+\right)\right\}\right]_L$$
$$+ \left[-\hbar g_{13}\left(a_1 - a_1^+\right)^2\left(a_2 + a_2^+\right) + \hbar g_{14}\left(a_2 + a_2^+\right)\left(a_2 - a_2^+\right)^2 - \hbar g_{15}\left(a_1 - a_1^+\right)\left(a_2 - a_2^+\right)\left(a_2 + a_2^+\right)\right.$$
$$\left.+ \hbar g_{16}\left(a_2 + a_2^+\right)^3 + i\hbar g_{17}\left(a_1 - a_1^+\right)\left(a_2 + a_2^+\right)^2 + i\hbar g_{18}\left(a_2 - a_2^+\right)\left(a_2 + a_2^+\right)^2\right]_{\mathrm{NL}}, \tag{10}$$

where $I_{\mathrm{P2'}} = I_{\mathrm{P2}} + I_{\mathrm{P2N}}$, $g_{12}' = g_{12} + g_{12\mathrm{N}}$, and $g_{22}' = g_{22} + g_{22\mathrm{N}}$. Also, $g_{13} = (1/2Z_1)(\sqrt{(\hbar/2Z_2)})g_{\mathrm{m2\_N}}C_{\mathrm{B}}{}^2/C_{\mathrm{M}}{}^4$, $g_{14} = (1/2Z_2)(\sqrt{(\hbar/2Z_2)})g_{\mathrm{m2\_N}}C_{\mathrm{C}}{}^2/C_{\mathrm{M}}{}^4$, $g_{15} = (1/\sqrt{(Z_2Z_1)})(\sqrt{(\hbar/2Z_2)})g_{\mathrm{m2\_N}}C_{\mathrm{B}}C_{\mathrm{C}}/C_{\mathrm{M}}{}^4$, $g_{16} = (Z_2/2)(\sqrt{(\hbar Z_2/2)})g_{\mathrm{m}}{}^2g_{\mathrm{m2\_N}}C_{\mathrm{B}}{}^2/C_{\mathrm{M}}{}^4$, $g_{17} = Z_2(\sqrt{(\hbar/2Z_1)})g_{\mathrm{m}}g_{\mathrm{m2\_N}}C_{\mathrm{B}}{}^2/C_{\mathrm{M}}{}^4$, and $g_{18} = Z_2(\sqrt{(\hbar/2Z_2)})g_{\mathrm{m}}g_{\mathrm{m2\_N}}C_{\mathrm{B}}C_{\mathrm{C}}/C_{\mathrm{M}}{}^4$. It is clearly shown in coefficients from g_{13} to g_{18} where the effect of $g_{\mathrm{m2\_N}}$ is dominant. In other words, the system's nonlinearity in this work is strongly changed and controlled by the second-order transconductance $g_{\mathrm{m2\_N}}$. Now, one can show using the total Hamiltonian of the system, which terms in the presented Hamiltonian in Eq. (10) can generate the squeezing state.

3. Results and discussions

A squeezed-coherent state is generally produced by the act of the squeezing and displacement operators on the vacuum state defined mathematically as $|\alpha,\zeta> = D(\alpha)S(\zeta)\ |0>$, where $|0>$ is the vacuum state[14]. It is found that the coher-

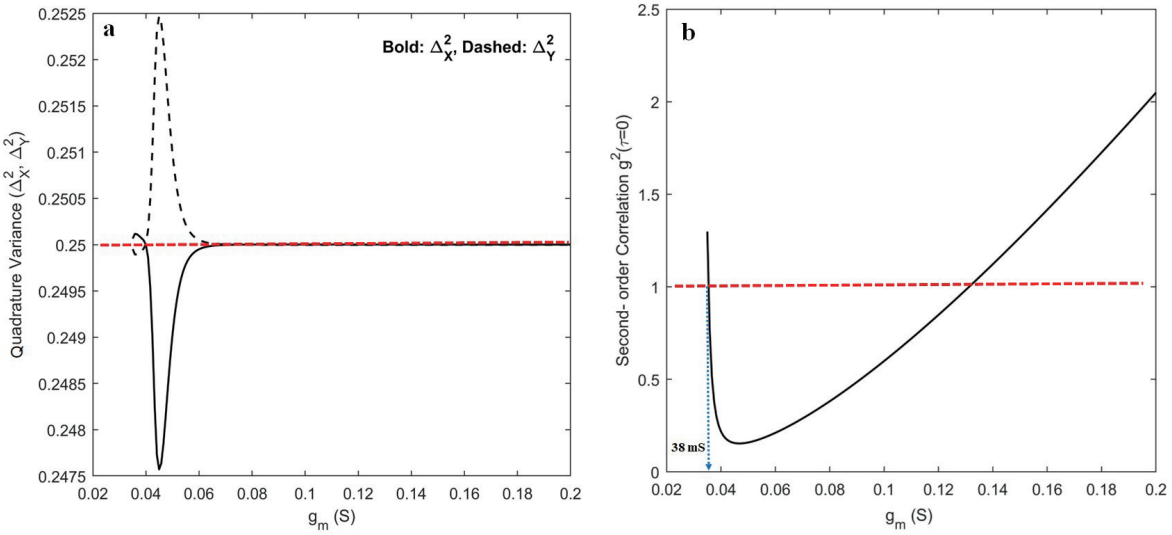

Fig. 3. (Color online) (a) Quadrature variance versus g_m. (b) Second-order correlation function versus g_m. C_f = 0.02 pF, g_{m3} = 1200 mA/V^3, g_{m2} = 200 mA/V^2, V_{RF} = 1 μV, $\kappa = \kappa_1 = \kappa_2 = 0.001\omega$.

ent state is generated by the linear terms in the Hamiltonian, whereas a squeezed state needs quadratic terms such as a^2 and a^{+2} in the exponent. The squeezed-coherent state $S(\zeta,\alpha)$ can be analyzed as the evolution $\exp[Ht/j\hbar]$ under the Hamiltonian defined in Eq. (10). Based on this definition, any quadratic terms such as a^2 and a^{+2} in the Hamiltonian may generate squeezing. The Hamiltonian in Eq. (10), the squeezed state, can be generated by:

$$S(\zeta) = \exp\left[\zeta_1\left(a_2^2 - a_2^{+2}\right) + \left(\frac{\zeta_2^*}{2}a_2^2 - \frac{\zeta_2}{2}a_2^{+2}\right)\right]t. \quad (11)$$

In this equation the squeezing parameters are defined as $\zeta_1 = -0.5g_{22}' + g_{18}\mathrm{Re}\{A_2\} + jg_{14}\mathrm{Im}\{A_2\}$ and $\zeta_2 = 2A_1^*(-g_{17} - jg_{15})$, where A_1 and A_2 are the strong fields (DC points) of LC_1 and LC_2. The DC points can be calculated using Heisenberg–Langevin equations in the steady-state[15, 16]. Also, Re{} and Im{} indicate the real and imaginary parts, respectively. Eq. (11) clearly shows that the squeezing is generated just for LC_2 and does not happen for LC_1. This point contributes to the nonlinearity terms in Hamiltonian expressed in Eq. (10) and also is related to the dependent current source containing g_{m2} and g_{m3}, which is directly connected to LC_2. The important point about the squeezing strength parameters ζ_1 and ζ_2 is that each depends on g_{m2_N}. In Eq. (11), ζ_1 and ζ_2 are complex numbers, meaning that the squeezing parameters contain the phase which determines the angle of the quadrature to be squeezed. Additionally, we found that the system can generate two-mode squeezing. That means that the nonlinearity created by the transistor couples two oscillators so that the coupled modes become squeezed. The expression generated due to the Hamiltonian of the system for two-mode squeezing is expressed as:

$$S_2(\zeta) = \exp\left[\left(\frac{\zeta_{t1}^*}{2}a_1a_2 - \frac{\zeta_{t1}}{2}a_1^+a_2^+\right) + \left(\frac{\zeta_{t2}^*}{2}a_1a_2 - \frac{\zeta_{t2}}{2}a_1^+a_2^+\right)\right]t, \quad (12)$$

where $\zeta_{t1} = jA_2g_{15}$ and $\zeta_{t2} = jA_1g_{13}$. In the same way, the squeezing parameters are strongly dependent on g_{m2_N}. Finally, one can easily find that the system can generate the coherent state, which means that the state generated by the Hamiltonian expressed in Eq. (10) is a squeezed-coherent state or a two-mode squeezed-coherent state. In the following, we just focus on the squeezed-coherent state and study the parameters that can manipulate the squeezing states. For simulation, the limit for time evolution in the exponent ($\exp[Ht/j\hbar]$) is defined as $t_0 < \{1/\kappa_1, 1/\kappa_2\}$, where κ_1 and κ_2 are the first and second oscillators' decay rates. By selecting t_0, the system is forced to generate squeezing before the resonator decaying, by which the squeezing is destroyed[1]. Some more information is introduced about t_0 in Appendix B.

In this study, quadrature variance is used to demonstrate the behavior of the state generated by the oscillators. In addition, we used the bunching and antibunching behavior of the generated photons. The second-order correlation function, $g^2(\tau)$, must be calculated. For the designed system, concerning the fact that t_0 limits the system, the photon counting time is sufficiently short. Thus, for such a short counting time, the variance of the photon number distribution is related to the second-order correlation function $g^2(\tau = 0) = 1 + (V(n) - \langle n\rangle)/\langle n\rangle$, where $V(n)$ and $\langle n\rangle$ are the photon number variance and the average, respectively[1, 13]. It has been shown that this phenomenon is called anti-bunching, a nonclassical phenomenon for light with sub-Poissonian statistics $g^2(\tau = 0) < 1$. Of course, $g^2(\tau = 0) < 1$ is not a necessary condition for squeezing the state; however, if $g^2(\tau = 0) > 1$, the field is a classical field[1]. In other words, the squeezing state may exhibit bunching and antibunching behaviors. The following section discusses the aforementioned points with some related simulations.

The squeezing of the second oscillator regarding Eq. (11) is simulated, and the results are shown in Fig. 3. As seen in Fig. 3(a), which illustrates the quadrature operator's variance versus g_m with the nominal reference of 0.25, the squeezing appears in the resonator and reaches the maximum value for g_m around 45 mS. However, the amount of the squeezing is decreased when g_m exceeds 60 mS. More clearly, the optimum amount of squeezing occurs between 38 and 60 mS. It may relate to the fact that g_m directly manipulates $\bar{I}_{ds}^2$ by which the noise exceeds in the system, and due to that, the squeezing is strongly limited when g_m is increased. Additionally, in Fig. 3(a), the dashed graph shows $\Delta y^2 > 0.25$, indicating that

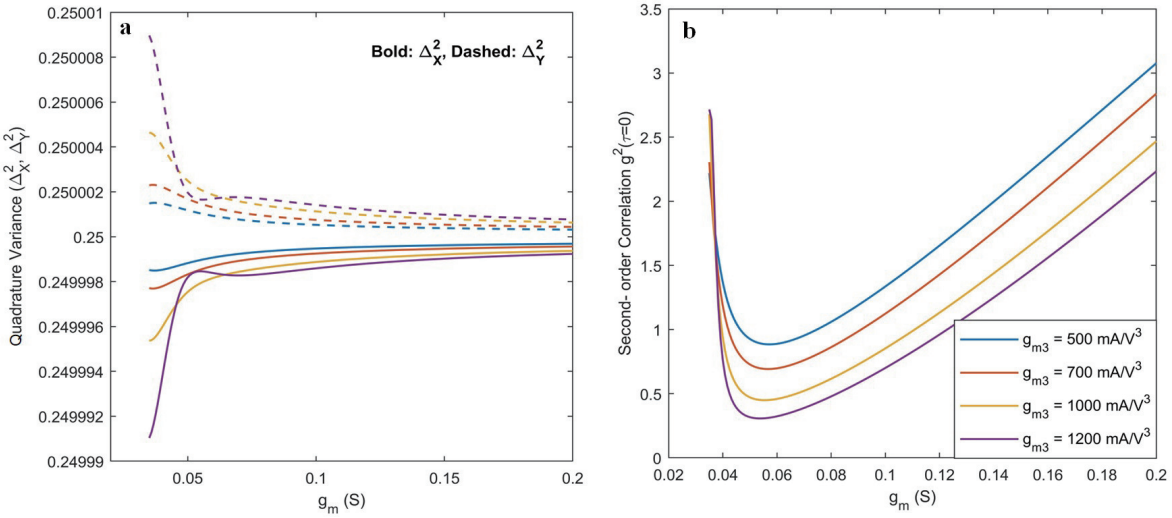

Fig. 4. (Color online) (a) Quadrature variance versus g_m, (b) second-order correlation function versus g_m for different g_{m3} (mA/V^3); C_f = 0.02 pF, g_{m2} = 200 mA/V^2, V_{RF} = 1 μV, $\kappa = 0.001\omega$.

this operator for each value of g_m shows bunching; in other words, the operator shows classical field behavior. We theoretically show that the important factors affecting LC_2 to generate a squeezing state include C_N, C_N', and g_{m2_N}. To know about the factor's effects and compare with other elements, the contributed values are calculated for g_m = 45 mS and represented as C_N = 3.3 pF, C_N' = 72 mA/V, and g_{m2_N} = 677 mA/V^2. These values show nonlinear effects in the transistor, which changes the electrical properties of the circuit. For instance, one can compare C_N with C_{gd} or C_{gs}, which indicates that C_N is greater than the internal capacitances and g_{m2_N} is comparable with g_{m2}.

In addition, the second-order correlation function $g^2(\tau = 0)$ behavior can be considered, as illustrated in Fig. 3(b). The figure shows perfect consistency with the quadrature operators' variance around g_m = 40 mS. The value of $g^2(\tau = 0)$ around 45 mS reaches its minimum and is less than 1, which means that the second resonator exhibits antibunching. Notably, the change in the sign of $g^2(\tau = 0)$ from bunching ($g^2(\tau = 0) > 1$) to antibunching ($g^2(\tau = 0) < 1$) indicates squeezing in the system. The results shown in Fig. 3(b) reveal that squeezing occurs only for small values of g_m. In other words, the transistor's current amplification factor (g_m) should be maintained at a low level to generate squeezing at cryogenic temperatures. Nonetheless, this is clearly shown in Eq. (11) that ζ_1 and ζ_2 are strongly manipulated by g_{m2_N}, which is a fundamental function of g_{m3}, and that C_N plays a key role in changing the coupling between resonators. Additionally, other factors such as feedback capacitance, LC resonator decay rate, and input RF source can influence the squeezing in the system. For instance, the effect of g_{m2}, g_{m3}, and that C_N plays a key role in changing the coupling between resonators. Additionally, other factors such as feedback capacitance, LC resonator decay rate, and input RF source can influence the squeezing in the system. For instance, the effect of g_{m3} as a nonlinearity factor on the quadrature operator variance and photon bunching and antibunching is illustrated in Fig. 4. Fig. 4(a) shows that by increasing $g_{m3,}$ the quadrature variance increases. This contributed to the increase in the squeezing strength parameters. In addition, the figure shows that increasing g_{m3} leads to maintaining $\Delta x^2 < 0.25$ for larger g_m. In the same way, the effect of g_{m3} increasing on the second-order correlation function is depicted in Fig. 4(b). This reveals that increasing g_{m3}, and that C_N plays a key role in changing the coupling between resonators. Additionally, other factors such as feedback capacitance, LC resonator decay rate, and input RF source can influence the squeezing in the system. For instance, the effect of g_{m3} causes an increase in g_m to 120 mS, in which the second-order correlation shows antibunching. This contributes to the fact that increasing g_{m3} changes C_N and g_{m2_N}, strengthening the squeezing behavior.

Additionally, the effects of other parameters such as C_f, V_{RF}, g_{m2}, and oscillator decay rate κ are analyzed in this study. The results of the simulations are depicted in Fig. 5. In this graph, the red dashed line is inserted to easily trace the bunching to the antibunching (and vice versa) entry point as a function of g_m. In this simulation, it is additionally, the effects of other parameters such as C_f, V_{RF}, g_{m2}, and oscillator decay rate κ are analyzed in this study. The results of the simulations are depicted in Fig. 5. In this graph, the red dashed line is inserted to easily trace the bunching to the antibunching (and vice versa) entry point as a function of g_{m3}, and that C_N plays a key role in changing the coupling between resonators. Additionally, other factors such as feedback capacitance, LC resonator decay rate, and input RF source can influence the squeezing in the system. For instance, the effect of g_m. In this simulation, it is assumed that the two oscillators had the same decay rate $\kappa_1 = \kappa_2 = \kappa$. As expected, Fig. 5 shows that increasing C_f, V_{RF}, and g_{m2} causes an increase in antibunching, whereas an increase in the decay rate leads to a decrease in antibunching. In this figure, the key factor that can be freely manipulated is the feedback capacitor, by which circuit properties, such as noise, gain, and stability, can be manipulated. The graph in Fig. 5(b) reveals that increasing the feedback capacitor causes antibunching for a larger g_m. This may be related to the noise figure enhancement using feedback in the circuit. In other words, using a feedback capacitor strongly enhances the noise figure of the circuit, which means that eliminating noise leads to enhanced squeezing. Assumed that the two oscillators had the same decay rate $\kappa_1 = \kappa_2 = \kappa$. As expected, Fig. 5 shows that increasing C_f, V_{RF}, and g_{m2} causes an increase in antibunching, whereas an increase in the decay rate

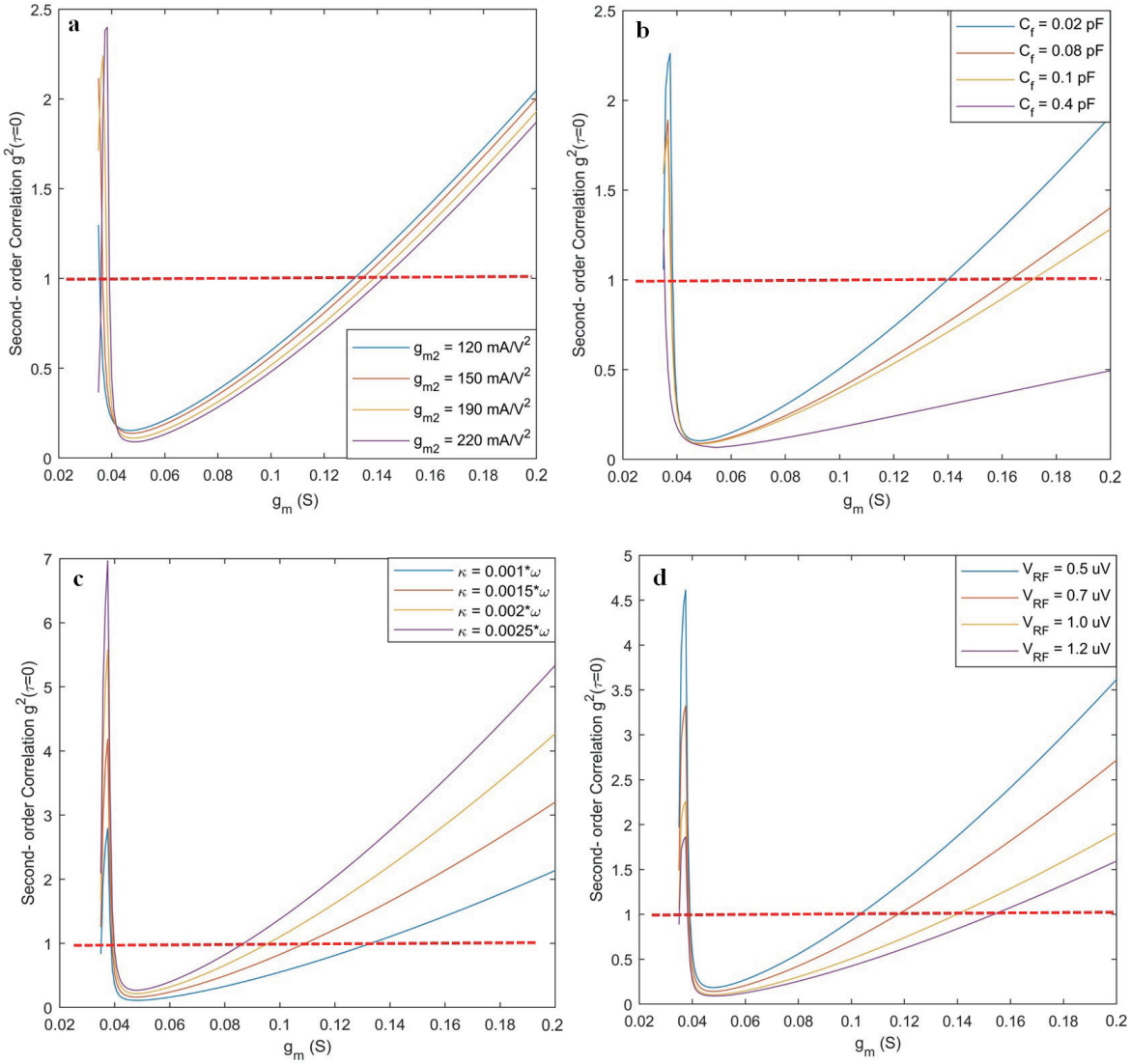

Fig. 5. (Color online) Second-order correlation function versus g_m. (a) g_{m2} effect. (b) Feedback capacitance effect (C_f). (c) LC resonator decay rate effect (κ). (d) Input RF source amplitude effect (V_{RF}). g_{m3} = 1200 mA/V^3.

leads to a decrease in antibunching. In this figure, the key factor that can be freely manipulated is the feedback capacitor, by which circuit properties, such as noise, gain, and stability, can be manipulated. The graph in Fig. 5(b) reveals that increasing the feedback capacitor causes antibunching for a larger g_m. This may be related to the noise figure enhancement using feedback in the circuit. In other words, using a feedback capacitor strongly enhances the noise figure of the circuit, which means that eliminating noise leads to enhanced squeezing.

The results illustrated in this study show that cryogenic InP HEMT transistor nonlinearity can generate a squeezed state. This is a significant achievement because such a system can be essential to a cryogenic detector used in quantum applications[29]. Thus, the operation of the detector or amplifier in the squeezed state implies that the noise fluctuation is limited below the zero-point changes. This is an interesting goal of this study; nonetheless, we know that this is challenging to achieve.

4. Conclusions

This article mainly emphasizes the generation of the squeezing state using the nonlinearity of the InP HEMT transistor. For this purpose, we designed a circuit containing two external oscillators coupled with a cryogenic InP HEMT transistor operating at 5 K. The circuit was analyzed using quantum theory, and the contributions of the Lagrangian and Hamiltonian functions were theoretically derived. Some key factors in the Hamiltonian arise because the transistor's nonlinearity could generate the squeezed state. Thus, we focused on these parameters and their engineering to generate squeezing. The results show that the squeezed state occurred only for the second oscillator. This implies that the first oscillator experiences a coherent state. In addition, we theoretically demonstrate that two coupled oscillators through a cryogenic transistor can generate two-mode squeezing. Thus, as a general point, if such a cryogenic circuit could generate squeezing, then the critical noise fluctuations would be minimal by which the coherent time of a quantum system is directly manipulated. Coherent time is the duration in which the entanglement can be created between modes. As a result, by optimizing this time through minimizing the noise in the system, the entanglement can be alive for a long time.

Appendix A

In this appendix, all of the parameters used in the main art-

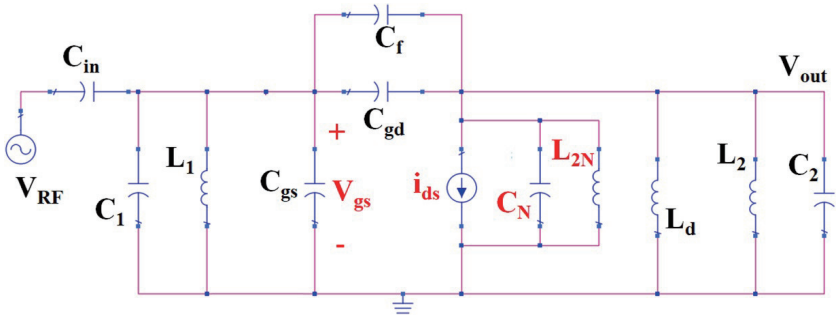

Fig. B1. (Color online) A simplified version of the circuit to estimate the transfer function.

icle listed as C_{q1}, C_{q2}, C_{q1q2}, g_{12}, g_{22}, V_{q1}, V_{q2} and I_{P2} are given by:

$$\frac{1}{C_{q1}} = \frac{2C_B^2(C_N + 0.5C_A)}{C_M^4} - \frac{C_C^2 C_B}{C_M^4},$$

$$\frac{1}{C_{q2}} = \frac{2C_C^2(C_N + 0.5C_A)}{C_M^4} + \frac{C_A{}^{i2} C_B}{C_M^4} - \frac{2C_C(C_N + C_A)C_B}{C_M^4},$$

$$\frac{1}{C_{q1q2}} = \frac{2C_C C_B(C_N + 0.5C_A)}{C_M^4} + \frac{C_C(C_N + C_A)C_B}{C_M^4} - \frac{C_C^2 C_B}{C_M^4},$$

$$\frac{1}{L_{p2}} = \frac{2g_m^2 C_B^2(C_N + 0.5C_A)}{C_M^4} + \frac{2g_m C_N' C_B}{C_M^2},$$

$$g_{12} = \frac{-2g_m C_B^2(C_N + 0.5C_A)}{C_M^4} + \frac{C_N' C_B}{C_M^2} - \frac{3g_m C_C^2 C_B}{2C_M^4},$$

$$g_{22} = \frac{-2g_m C_B C_C(C_N + 0.5C_A)}{C_M^4} + \frac{C_N' C_C}{C_M^2} + \frac{g_m C_C^3}{C_M^4} - \frac{g_m(C_N + C_A)C_C C_B}{C_M^4},$$

$$V_{q1} = \frac{2C_B C_C C_{in} V_{RF}(C_N + 0.5C_A)}{C_M^4} - \frac{C_C^2 C_{in} C_B V_{RF}}{C_M^4},$$

$$V_{q2} = \frac{2C_B C_C C_{in} V_{RF}(C_N + 0.5C_A)}{C_M^4} - \frac{C_C^3 C_{in} V_{RF}}{C_M^4},$$

$$I_{p2} = \frac{-2g_m C_B^2 C_{in} V_{RF}(C_N + 0.5C_A)}{C_M^4} + \frac{g_m C_B C_{in} C_C^2 V_{RF}}{C_M^4} - \frac{C_B C_{in} C_N' V_{RF}}{C_M^2} - \overline{I_{ds}{}^2},$$

where and $C_N' = 2g_{m2}(\partial\varphi_i/\partial t)|_{dc} + 12g_{m3}[(\partial\varphi_i/\partial t)|_{dc}]^2$.

Appendix B

In this appendix, we try to give some information about t_0. The main article discusses that t_0 is selected less than the times that two oscillators decay with it. In fact, from a classical point of view, t_0 should be in the order of the steady-state time. Therefore, in this part, we tried to calculate the step response of the circuit. For this reason, however, for simplicity, a simplified version of the circuit shown in Fig. 2 is demonstrated in Fig. B1 (Dip Trace software is used to draw the schematic), and the related transfer function is derived as:

$$\frac{V_{out}(s)}{V_{RF}(s)} = \frac{g_m L_{p2} L_1 S^2}{L_{p2}L_1 C_{p1} C_{p2} S^4 + L_{p2} L_1 C_{p2} S^3 + (L_1 C_{p1} + L_{p2} C_{p2}) S^2 + L_1 S + 1}, \quad \text{(B1)}$$

where $L_{p2} = L_{2N}||L_2$, $C_{p1} = C_{gs} + C_1 + (C_{gd} + C_f)A_{v0}$, $C_{p2} = C_N + C_2$. As can be seen in the expressions, the second oscillator's inductance and capacitance are affected by the nonlinearity effects as L_{2N} and C_N, and the first oscillator is just influenced by the gain of the circuit A_{v0}–$g_m r_0$, where r_0 is the resistance generated due to the channel length modulated effect. The step response of the transfer function expressed in Eq. (B1) is illustrated in Fig. B2. It is shown that the settling time is around 80 ns; this time is very close to t_0, which we selected based on the oscillator's decay rates. In fact, t_0 is selected around the settling time for the system.

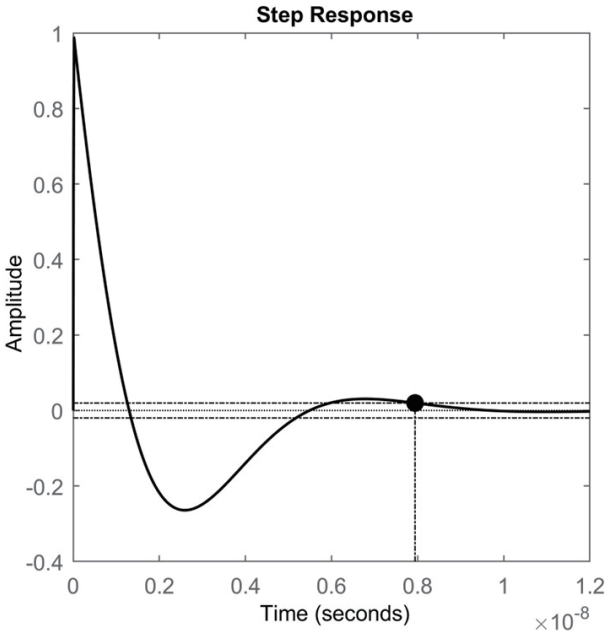

Fig. B2. Step response of the circuit.

References

[1] Walls D F. Squeezed states of light. Nature, 1983, 306, 141
[2] Mandel L. Squeezed states and sub-poissonian photon statistics. Phys Rev Lett, 1982, 49, 136
[3] Rodrigues H, Portes D Jr, Duarte S B, et al. Squeezing in coupled oscillators having neither nonlinear terms nor time-dependent parameters. Braz J Phys, 2001, 31, 562
[4] Friberg S, Mandel L. Production of squeezed states by combination of parametric down-conversion and harmonic generation. Opt Commun, 1984, 48, 439
[5] Mollow B R, Glauber R J. Quantum theory of parametric amplification. I. Phys Rev, 1967, 160, 1076
[6] Shahriar M S, Hemmer P R. Generation of squeezed states and twin beams via non-degenerate four-wave mixing in a Λ system. Opt Commun, 1998, 158, 273
[7] Lvovsky A I. Squeezed light. In: Photonics: Scientific foundations, technology and applications. John Wiley & Sons, Inc, 2015, 121
[8] Yuen H P, Shapiro J H. Generation and detection of two-photon co-

herent states in degenerate four-wave mixing. Opt Lett, 1979, 4, 334
[9] Hirano T, Matsuoka M. Broadband squeezing of light by pulse excitation. Opt Lett, 1990, 15, 1153
[10] Breitenbach G, Schiller S, Mlynek J. Measurement of the quantum states of squeezed light. Nature, 1997, 387, 471
[11] Yamamoto Y, Machida S, Richardson W H. Photon number squeezed states in semiconductor lasers. Science, 1992, 255, 1219
[12] Raiford M T. Statistical dynamics of quantum oscillators and parametric amplification in a single mode. Phys Rev A, 1970, 2, 1541
[13] Davidovich L. Sub-Poissonian processes in quantum optics. Rev Modern Phys, 1996, 68, 127
[14] Scully M O, Zubairy M S. Quantum Optics. Cambridge: : Cambridge University Press, 1997
[15] Salmanogli A, Gokcen D. Entanglement sustainability improvement using optoelectronic converter in quantum radar (interferometric object-sensing). IEEE Sens J, 2021, 21, 9054
[16] Salmanogli A, Gokcen D, Gecim H S. Entanglement sustainability in quantum radar. IEEE J Sel Top Quantum Electron, 2020, 26, 1
[17] Barzanjeh S, Pirandola S, Vitali D, et al. Microwave quantum illumination using a digital receiver. Sci Adv, 2020, 6, eabb0451
[18] Barzanjeh S, Guha S, Weedbrook C, et al. Microwave quantum illumination. Phys Rev Lett, 2015, 114, 080503
[19] Salmanogli A, Gokcen D. Design of quantum sensor to duplicate European Robins navigational system. Sens Actuat A Phys, 2021, 322, 112636
[20] Salmanogli A, Gokcen D, Gecim H S. Entanglement of optical and microcavity modes by means of an optoelectronic system. Phys Rev Appl, 2019, 11, 024075
[21] Aparin V, Larson L E. Modified derivative superposition method for linearizing FET low-noise amplifiers. IEEE Trans Microwave Theory Techn, 2005, 53, 571
[22] Ganesan S, Sanchez-Sinencio E, Silva-Martinez J. A highly linear low-noise amplifier. IEEE Trans Microwave Theory Techn, 2006, 54, 4079
[23] Hamaizia Z, Sengouga N, Missous M, et al. A 0.4dB noise figure wideband low-noise amplifier using a novel InGaAs/InAlAs/InP device. Mater Sci Semicond Process, 2011, 14, 89
[24] Yurke B, Roukes M L, Movshovich R, et al. A low-noise series-array Josephson junction parametric amplifier. Appl Phys Lett, 1996, 69, 3078
[25] Schleeh J, Alestig G, Halonen J, et al. Ultralow-power cryogenic InP HEMT with minimum noise temperature of 1 K at 6 GHz. IEEE Electron Device Lett, 2012, 33, 664
[26] Cha E, Wadefalk N, Moschetti G, et al. A 300-μW cryogenic HEMT LNA for quantum computing. 2020 IEEE/MTT-S International Microwave Symposium (IMS), 2020, 1299
[27] Wadefalk N, Mellberg A, Angelov I, et al. Cryogenic wide-band ultra-low-noise if amplifiers operating at ultra-low DC power. IEEE Trans Microwave Theory Techn, 2003, 51, 1705
[28] Salmanogli A, Gecim H S. Design of the ultra-low noise amplifier for quantum applications. arXiv preprint arXiv: 2111.15358, 2021
[29] Salmanogli A. Entangled microwave photons generation using cryogenic low noise amplifier (transistor nonlinearity effects). Quantum Sci Technol, 2022, 7, 045026
[30] Fan X H, Zhang H, SÁnchez-Sinencio E. A noise reduction and linearity improvement technique for a differential cascode LNA. IEEE J Solid State Circuits, 2008, 43, 588
[31] Cha E, Moschetti G, Wadefalk N, et al. Two-finger InP HEMT design for stable cryogenic operation of ultra-low-noise Ka-and Q-band LNAs. IEEE Trans Microwave Theory Tech, 2017, 65, 5171-80
[32] Cha E, Wadefalk N, Moschetti G, et al. InP HEMTs for sub-mW cryogenic low-noise amplifiers. IEEE Electron Device Lett, 2020, 41, 1005
[33] Mellberg A, Wadefalk N, Angelov I, et al. Cryogenic 2-4 GHz ultra low noise amplifier. 2004 IEEE MTT-S International Microwave Symposium Digest, 2004, 161

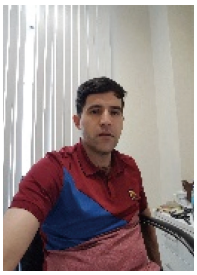

Ahmad Salmanogli received his B.S. and M.Sc. degrees in Electrical Engineering from Tabriz University and his Ph.D. degree in electrical and electronics engineering from Hacettepe University in 2021. His research interests include quantum electronics, circuit QED, quantum radar, and quantum-RF circuit designing such as cryogenic LNA.